Preparation and properties of Y_2O_3-doped ZrO_2 thin films by the sol–gel process

JOO-SIN LEE
Department of Materials Science and Engineering, Kyung-Sung University, Nam-gu, Pusan, 608-736, Korea

T. MATSUBARA, T. SEI, T. TSUCHIYA
Department of Materials Science and Engineering, Science University of Tokyo, Noda-shi, Chiba, 278, Japan

Y_2O_3-doped ZrO_2 (YZ) thin films were prepared on alumina substrates by the dip-coating process. The dip-coating solution consisted of a homogeneous sol, and was prepared by using the respective chlorides as raw materials, with ethylene glycol, 2-butanol and distilled water as solvents. The thin films containing 0–20 mol % Y_2O_3 were successfully produced by thermal treatment above 600 °C. The characterization for the film preparation was performed by means of thermogravimetric–differential thermal analysis for the thermal analysis, and scanning electron microscopy for the morphological analysis and thickness measurements. The properties of the films were characterized in terms of a study of the crystalline phase, the crystallite size, the microstructure and the electrical conductivity by using X-ray diffraction, scanning electron microscopy and the complex impedance techniques. In all YZ thin films, the tetragonal phase was stable at low temperatures as a result of the crystallite size effect. However, at higher temperatures, the tetragonal phase was transformed into either the monoclinic phase or the cubic phase, depending on the doping concentration. The YZ thin film of 8 mol % Y_2O_3 content was stabilized to almost cubic phase at 1000 °C. Resonable conductivity behaviour at YZ was observed for the YZ thin films. The electrical conductivity of YZ thin films was similar to the values of the sintered body.

1. Introduction

Y_2O_3-doped ZrO_2 is widely used for structural materials because of a number of superior properties, such as heat resistance, high hardness, and chemical durability, and for electronic materials using the oxygen ionic conductivity. Using these properties, the dense thin films are applied in fuel cells, oxygen sensors, and films for corrosion resistance and heat resistance against oxidation.

In all these applications, the polymorphic stability of zirconia over a broad temperature range is very important. It is well known that zirconia shows three phases with increasing temperatures, e.g. monoclinic up to ~1170 °C, tetragonal up to ~2370 °C and cubic up to the melting temperature, at ~2706 °C. The stabilization of the high-temperature phases at moderate temperatures ensures the excellent mechanical, thermal, and electrical properties of zirconia ceramics.

The coatings of pure ZrO_2 [1–6] and Y_2O_3-doped ZrO_2 [7–13] produced by the sol–gel process have been researched for several years, because of several advantages, such as low processing temperatures, homogeneity, the possibility of coating on substrates with large areas, and low cost.

Negishi [7] prepared zirconia and stabilized-zirconia thin films by the thermal decomposition process of painted films of zirconium 2-ethylhexonate and yttrium 2-ethylhexonate. He showed that the process is applicable to fuel cells and sensors by the thin solid electrolyte film technique.

Peshev *et al.* [10] also reported the preparation of thin yttria-stabilized zirconia films by using an isopropanol sol of zirconium propoxide and yttrium isopropoxide. Crack-free yttria-stabilized zirconia films, approximately 0.2–0.5 μm thick, were deposited on continuous quartz substrates by Kueper *et al.* [11]. Sakurai *et al.* [12] also reported the coatings of 8.8 mol % yttria-doped zirconia, fabricated using hydrolysis of zirconium *n*-butoxide and yttrium nitrate.

The above reports were attempts to prepare stabilized zirconia thin film for application to the solid electrolyte [7, 10–12]. There are other reports in the literature of the application of the chemical protection of metal substrates from attack by acid and oxidation [3, 4, 6, 8, 9, 13].

Studies on pure ZrO_2 thin-film preparation, using several organozirconium compounds by Izumi *et al.* [3], and zirconium isopropoxide by Neto *et al.* [4] and Atik *et al.* [6], reported that the heat resistance

0022–2461

against oxidation [3] and chemical corrosion resistance [4, 6] were improved by the ZrO_2 coating on stainless steel sheets.

Shane *et al.* [8] reported that 8 wt % Y_2O_3–ZrO_2 was prepared by spin-coating a solution containing zirconium alkoxides and yttrium acetate on stainless steel substrates. In addition, stabilized ZrO_2 thin films were prepared by Maggio *et al.* [9] using zirconium tetra-*n*-tuboxide and cerium (III)-2-4-petanedionate for CeO_2–ZrO_2, and by Miyazawa *et al.* [13] using zirconium tetra-*n*-butoxide and yttrium acetate tetrahydrate for Y_2O_3–ZrO_2.

Until now, the starting materials for the sol–gel thin films have usually used the metal alkoxides [1–13]. However, these materials are expensive and they exhibit differences in the hydrolysis rate of each component. There has been very limited attention directed at the preparation of stabilized zirconia thin films by using the non-alkoxides as starting materials and the systematic study of the variation of the stabilizer content.

In this work, the inorganic salts which have not usually been used, were used as starting materials to fabricate the Y_2O_3-doped ZrO_2 (YZ) thin films. The characterization for the thin-film fabrication, such as the thermal analysis, morphological analysis and thickness measurements, was performed. The properties of thin films were also evaluated through phase analysis, microstructure analysis, and electrical conductivity measurements.

2. Experimental procedure

The thin films prepared in this study have the composition of $(100 - x)ZrO_2 \cdot xY_2O_3$, where $x = 0$, 2, 5, 8, 11 and 20, respectively. Fig. 1 shows the procedures for YZ thin-film processing. Zirconium chloride octahydrate ($ZrOCl_2 \cdot 8H_2O$) powder (Wako Pure Chemical Industries, Ltd, Japan, purity 99%) and yttrium chloride hexahydrate ($YCl_3 \cdot 6H_2O$) powder (Wako Pure Chemical Industries, Ltd, Japan, purity 99.9%) were used as raw materials, which were dissolved in the mixed solvents of ethylene glycol, 2-butanol and distilled water. They were stirred at room temperature and dissolved to form a coating solution. A homogeneous and transparent sol was obtained. A commercial alumina plate was used as a substrate. The substrates were degreased ultrasonically in acetone before dipping. The substrate was dipped into the solution and withdrawn at a rate of about 1 cm min^{-1}.

The coated substrate was calcined at 600 °C for 2 h and then heat treated at each given temperature for 2 h at a heating rate of 5 °C min^{-1}. Calcining and heat treatment were performed in air. The coating and calcining processes were repeated five times to obtain a sufficient thickness for measurements of properties. The thickness of the films dipped five times was about 0.6 μm.

Characterization for the film preparation was performed by means of thermogravimetric analysis (TG), differential thermal analysis (DTA), and scanning electron microscopy (SEM). Thermal analysis was

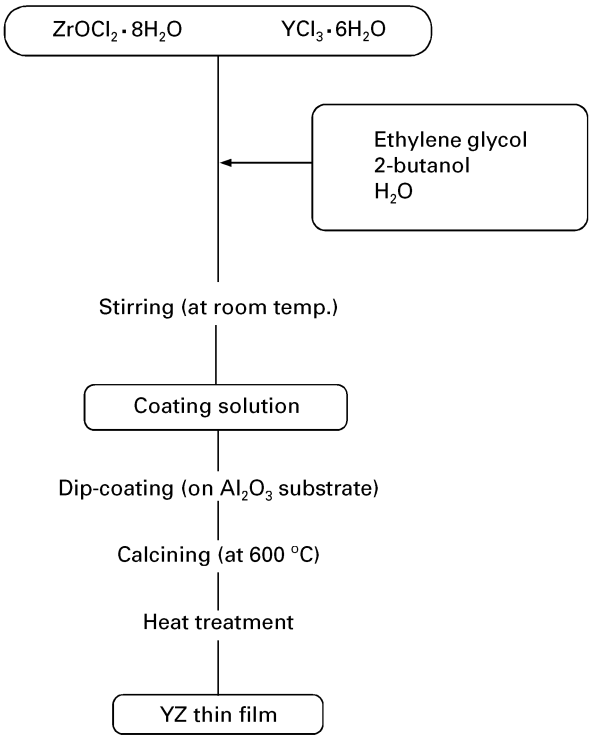

Figure 1 Preparation procedure for YZ thin film.

performed on dried powders of the coating solution at a heating rate of 5 °C min^{-1} by using TG and DTA (Rigaku type 8078). Film thickness was determined by SEM (Jeol JSM-T100) observation of the fractured surface of specimens.

The as-coated films were characterized to study the crystalline phase, the crystallite size, the microstructure and the electrical conductivity. The phase transitions during heat treatments were studied by X-ray diffraction (XRD) using CuK_α radiation. The X-ray diffractometer (Rigaku CN4148) was equipped with a thin-film attachment and a carbon monochromator. The X-ray diffraction patterns were recorded in the range $20° < 2\theta < 80°$. Lattice constants were calculated from the *d*-spacing of the (1 1 1) diffraction peak measured by XRD. α-Al_2O_3 was used as a reference.

For the estimation of crystallite sizes as a function of heat-treatment temperature, X-ray diffraction-line broadening (XRD-LB) measurements were performed. The Scherrer equation was used for the calculation:

$$D = \frac{k\lambda}{B\cos\theta} \tag{1}$$

where D is the crystallite size (nm), λ is the wavelength of CuK_α radiation (nm), θ is the Bragg angle (deg), k is a constant, 0.89, and B is the calibrated width of a diffraction peak at half-maximum intensity (rad). Assessments of crystallite size of the thin film were also obtained from the SEM observations.

The electrical conductivity was measured by the complex impedance method at 100 Hz to 15 MHz using an impedance analyser (Hewlett Packard impedance/gain-phase analyser 4194A). A comb pattern of

electrodes was screen-printed on the coating surface using platinum paste (Tokuriki Chemical Research and Development). The platinum paste was baked at 1000 °C for 10 min.

The electrical conductivity $\sigma(\mathrm{S\,cm^{-1}})$ was calculated from Equation 2

$$\sigma = \frac{l}{RtNL} \tag{2}$$

where R (Ω) is the resistance obtained from Nyquist diagrams in which the imaginary impedance is plotted against the real impedance, t (cm) is the film thickness, N is the number of electrode pairs in the comb pattern, L (cm) is the length of electrodes, and l (cm) is the separation distance of electrodes.

3. Results and discussion

Fig. 2 shows TG and DTA curves for the dried powders of 8 mol % YZ coating solution. The coating solution was dried at 200 °C for 24 h. Endothermic and exothermic peaks were found with weight loss until 500 °C, and no other thermal effect was observed above this temperature. Their origins may be attributed to the evaporation of solvents or burning of organic compounds.

An exothermic peak at around 350 °C can be attributed to the crystallization of zirconia. This was confirmed by the XRD data. All dried samples containing 0–20 mol % Y_2O_3 exhibit similar DTA curves. From the results of TG and DTA data, the calcination temperature was determined as 600 °C, with no other thermal effects being observed above this temperature.

Fig. 3 shows scanning electron micrographs of 8 mol % YZ film heat treated at 1000 °C for 2 h. The film was coated five times. A dense film uniformly coated on an alumina substrate is shown. The thickness of the film coated five times is about 0.6 μm. As shown in Fig. 3b, the film is crack-free and consists of densely packed crystallites with a diameter of about 50 nm. Good uniformity in crystallite size is also shown.

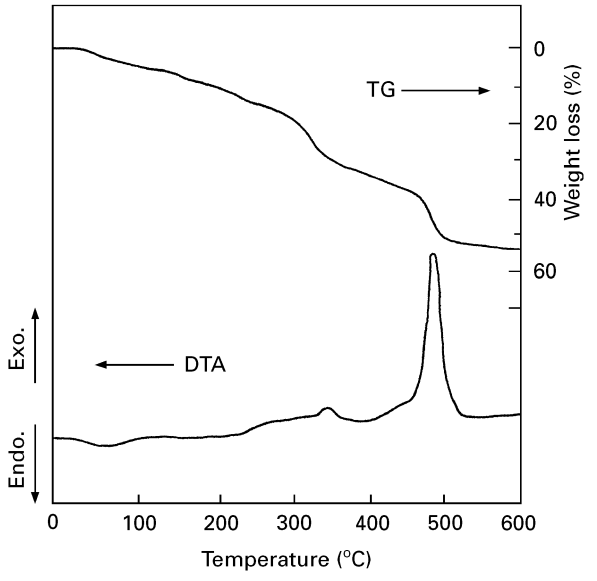

Figure 2 TG and DTA curves for the dried powders of 8 mol % YZ coating solution.

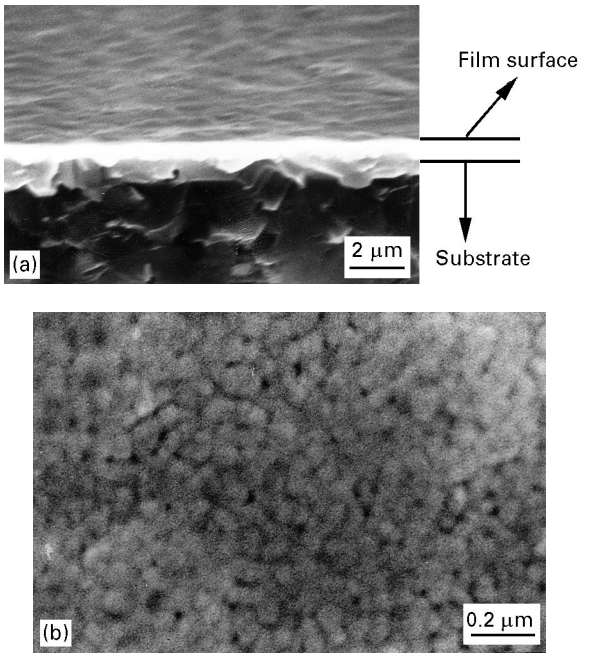

Figure 3 Scanning electron micrographs of 8 mol % YZ film heat treated at 1000 °C for 2 h: (a) cross-section, (b) surface.

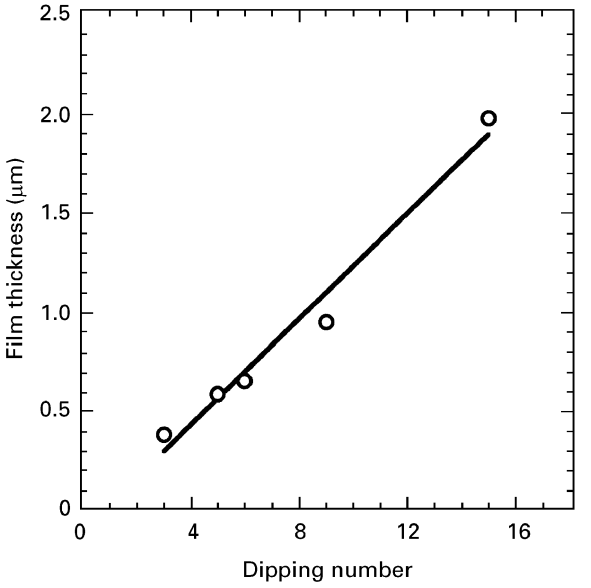

Figure 4 Film thickness as a function of the number of dippings.

The film thickness increases linearly as the number of dippings increases, as shown in Fig. 4. This confirms that thickness can be easily controlled by the number of dippings. A film thickness of about 0.12 μm was obtained by each dip-coating. We know that a film thickness of submicrometre order can be controlled by the sol–gel method, although the electrochemical vapour deposition (EVD) process mainly studied for solid-oxide fuel-cell applications [14, 15] can produce a thickness of micrometre order.

Fig. 5 shows X-ray diffraction patterns of pure ZrO_2 thin film obtained from different thermal treatments. The open circles in this figure show the peaks

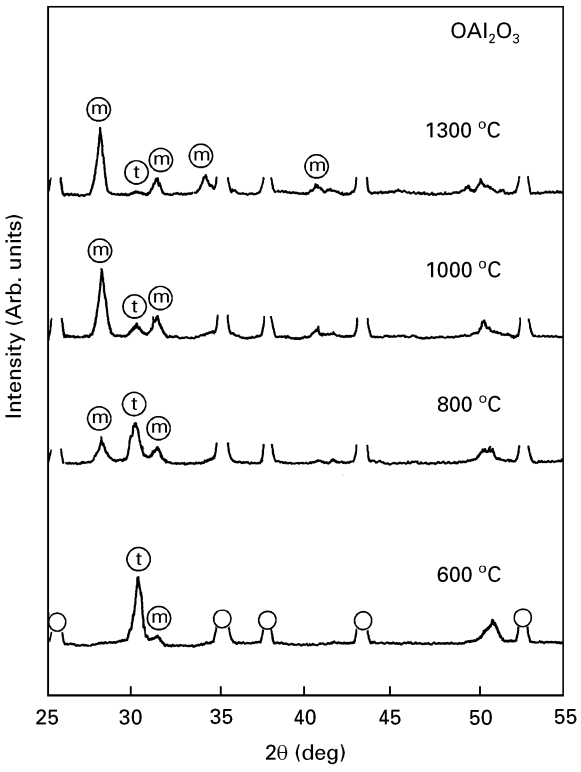

Figure 5 XRD patterns of ZrO_2 thin film heat treated at various temperatures for 2 h.

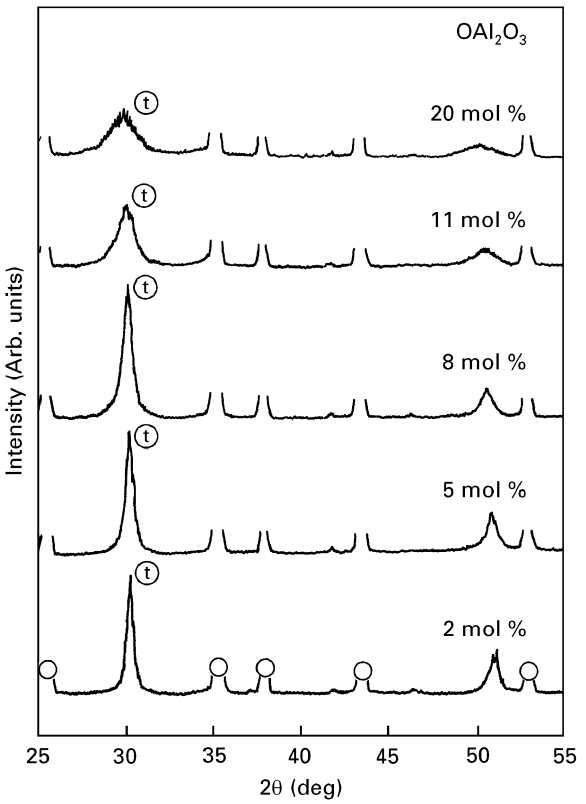

Figure 6 XRD patterns of YZ thin film heat treated at 600 °C for 2 h.

from the alumina substrate. In the figure, t and m denote the tetragonal phase and the monoclinic phase, respectively. At 600 °C, the main peak (1 1 1 plane) of tetragonal phase is shown with a very weak peak of monoclinic phase. With increasing temperature, the intensity of the tetragonal peaks decreases, and the monoclinic phase is largely formed. The orderly progression of the phase transition is observed with increasing temperature.

It is known that for the zirconia having small crystallite size, the metastable tetragonal phase exists at low temperatures as a result of the crystallite size effect [16]. The crystallite sizes of thin films obtained in this study are smaller than 30 nm, the critical size of the crystallite size effect (see Fig. 3b and Fig. 11 below). For thin films having crystallite sizes below 30 nm, the results of Fig. 5 are reasonable.

Figs 6–8 show the film composition dependence of the X-ray diffraction patterns in the YZ specimens, heat treated at 600, 1000 and 1300 °C, respectively. All the YZ thin films heat treated at 600 °C have the tetragonal phase, as shown in Fig. 6. This coincides with the stabilization of the tetragonal phase at low temperatures. Fig. 6 is characteristic of the trend of peak broadening with increasing yttria content. The similar tendency is observed up to the XRD data of YZ heat treated at 800 °C; however, no such tendency is observed above this temperature (see Figs 7 and 8).

These phenomena can be related to the crystallization behaviour, which is strongly influenced by the yttria content. In a detailed study of the dehydration and crystallization behaviour of zirconia–yttria gels obtained by coprecipitation, Ramanathan *et al.* [17] reported that a sharp exothermic peak in the DSC

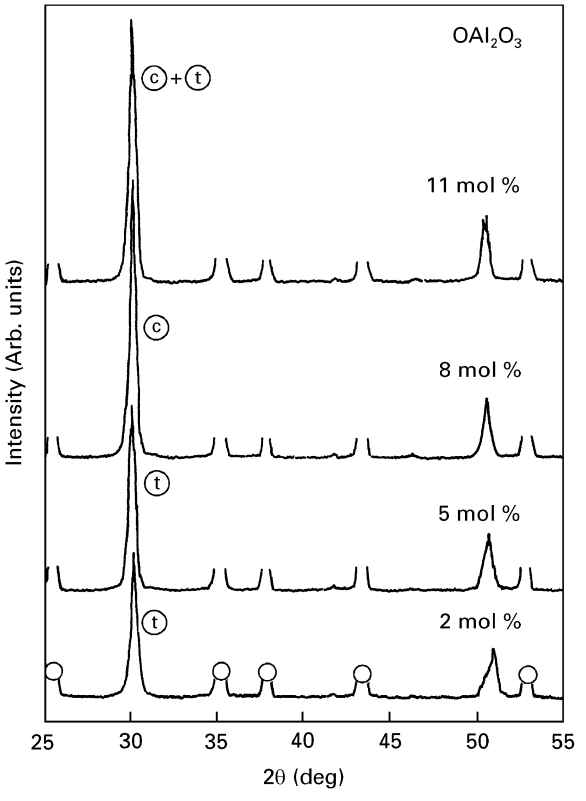

Figure 7 XRD patterns of YZ thin film heat treated at 1000 °C for 2 h.

profiles due to the crystallization of zirconia was drastically reduced by increasing the yttria content. They also showed that the temperature of the crystallization peak was shifted to higher temperatures with an

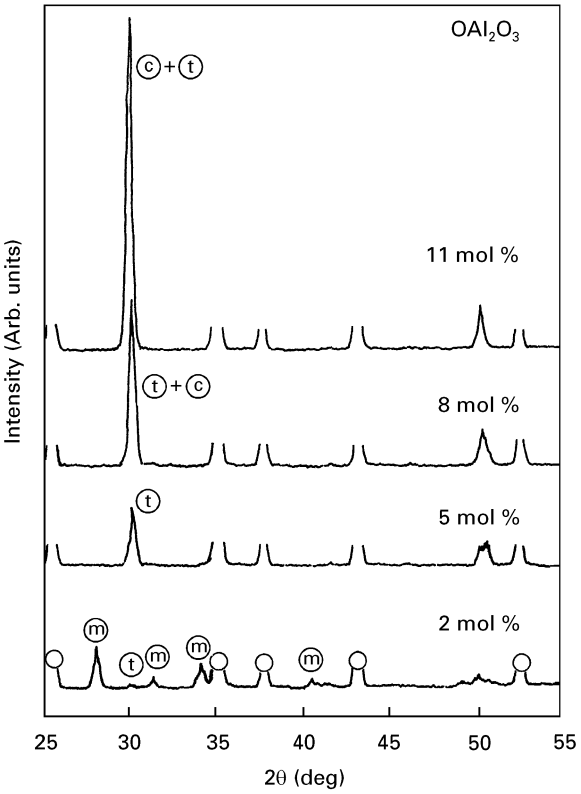

Figure 8 XRD patterns of YZ thin film heat treated at 1300 °C for 2 h.

increase in the yttria content, while the activation energy and kinetic constant were increased.

Fig. 7 shows XRD patterns of YZ thin film heat-treated at 1000 °C (c denotes the cubic phase). The angle dependence of all XRD patterns is very similar at 1000 °C, showing the tetragonal phase and/or the cubic phase. From the high-angle pattern of XRD, we can easily discriminate between tetragonal and cubic phases [18] as shown in Fig. 9, even though the angles of the diffraction peaks due to cubic phase overlap with the peaks from the tetragonal phase in the low angles below $2\theta = 72^\circ$. The cubic phase was seen in the lower-angle region of the high-angle XRD patterns of the range $2\theta = 68^\circ$–78°. In the figure, $(400)_c$ and $(400)_t$ denote the cubic phase and the tetragonal phase, respectively.

From these results, it can be seen that, at the lower doping concentrations, only the tetragonal phase exists, while the cubic plus tetragonal phases exist at the higher doping concentrations. In particular, there is a feature of the dominant cubic phase in the YZ of 8 mol % Y_2O_3 content. It is well known that the amount of dopant required to stabilize fully the cubic structure is about 8–9 mol % for Y_2O_3, and the conductivity maximum in the electrical conductivity–dopant concentration curves also corresponds to this amount [19].

As the temperature of heat treatment is increased, YZ of 2 mol % Y_2O_3 content shows the monoclinic behaviour, as shown in Fig. 8. This is qualitatively similar to the pure ZrO_2 data of Fig. 5, even though the temperature of the phase transition is dependent on the doping concentration. With increasing yttria content the main peak of the tetragonal and/or cubic

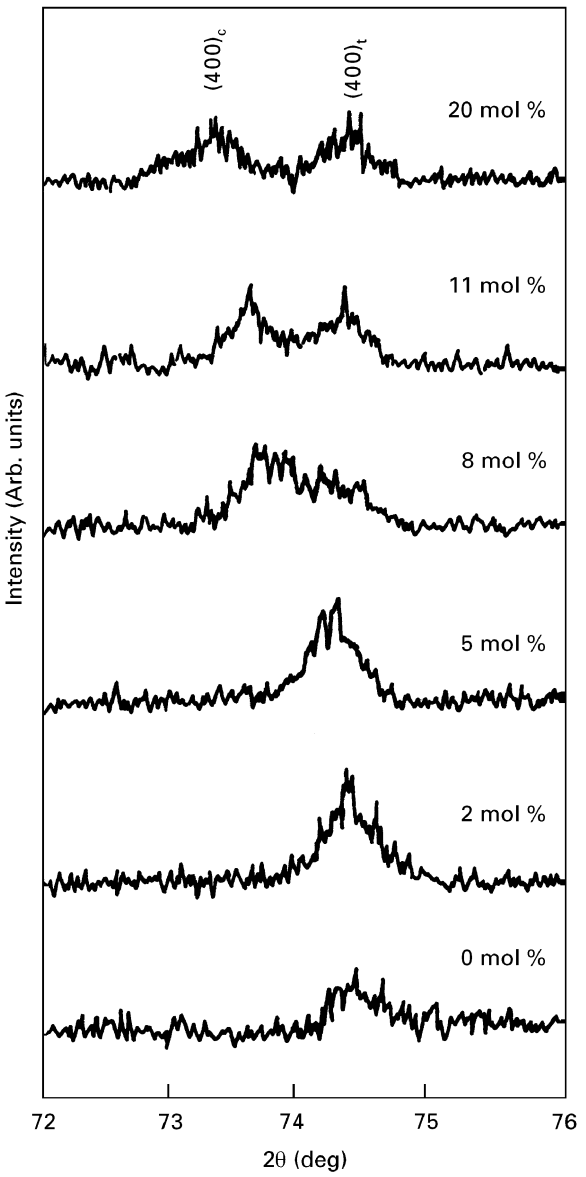

Figure 9 High-angle XRD patterns of YZ thin film heat treated at 1000 °C for 2 h.

TABLE I Phase transitions of YZ thin films heat treated at various temperatures

Y_2O_3 content (mol %)	Heat-treatment temperature			
	600 °C	800 °C	1000 °C	1300 °C
0	t + [m][a]	t + (m)[b]	m + (t)[b]	m + [t][a]
2	t	t	t + [m][a]	m + (t)[b]
5	t	t	t	t + (m)[b]
8	t	t + c	c + (t)[b]	t + c
11	t	t + (c)[b]	c + t	c + t
20	t	t	c + t	c + t

[a] Very small
[b] Small

phases is grown, and the cubic phase becomes dominant.

The phase transitions of YZ thin films are summarized in Table I. Notations t, m, and c denote the tetragonal phase, the monoclinic phase and the cubic phase, respectively. For all the YZ thin films, the

tetragonal phase is stable at low temperatures as a result of the crystallite size effect. At the higher temperatures, the tetragonal phase is transformed into either the monoclinic phase or the cubic phase, depending on the doping concentration.

At the lower doping concentrations, the tetragonal phase is transformed into the monoclinic phase. With increasing doping concentration, the transition temperature of monoclinic phase becomes higher. This is the result of the stabilization of tetragonal phases, due to the addition of a stabilizer [20]. A YZ thin film of 5 mol % Y_2O_3 content shows the tetragonal phase over all the heat-treatment temperatures in this study.

However, at higher doping concentrations, the tetragonal phase of low temperatures is transformed into the cubic phase. YZ thin film of 8 mol % Y_2O_3 content is stabilized to almost cubic phase at 1000 °C. Also, an increase in the content of tetragonal phase is observed at 1300 °C.

Sakurai *et al.* [12] reported similar results in 8.8 mol % yttria-doped zirconia coatings prepared by the hydrolysis of zirconium alkoxide with hydrogen peroxide and nitric acid. They obtained the cubic phase after heating at 1000 and 1200 °C, and the cubic and tetragonal phases at 1350 °C. They explained the results from the fact that the partial transformation to the tetragonal phase is probably due to the diffusion of yttrium into the grain boundary and/or into the alumina substrate.

Fig. 10 shows the compositional dependence of lattice constants in the system of YZ heat treated at 1000 °C. The closed and open circles represent the lattice constants of the *a*-axis and *c*-axis, respectively. The lattice constants of *a*-axis and *c*-axis overlap with increasing yttria content, which reveals the phase transitions from the tetragonal phase into the cubic phase. This result is in good agreement with the third column of Table I. Another feature is the increase in lattice constants with the yttria content. This suggests that yttrium ions are distributed uniformly in the solid solution of cubic zirconia. The radius of the yttrium ion is bigger than that of the zirconium ion (Y^{3+} 0.096 nm, Zr^{4+} 0.082 nm).

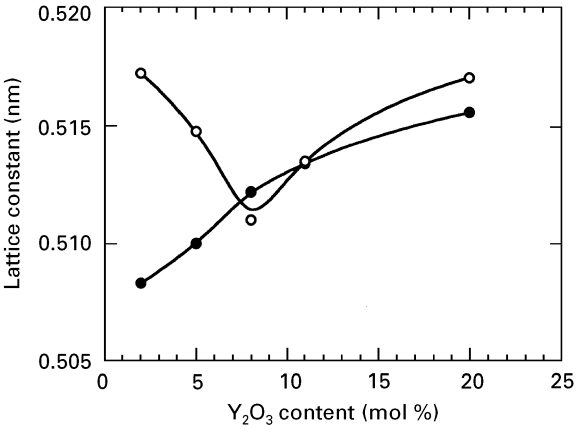

Figure 10 Lattice constants of YZ thin film heat treated at 1000 °C for 2 h: (○) *c*-axis, (●) *a*-axis.

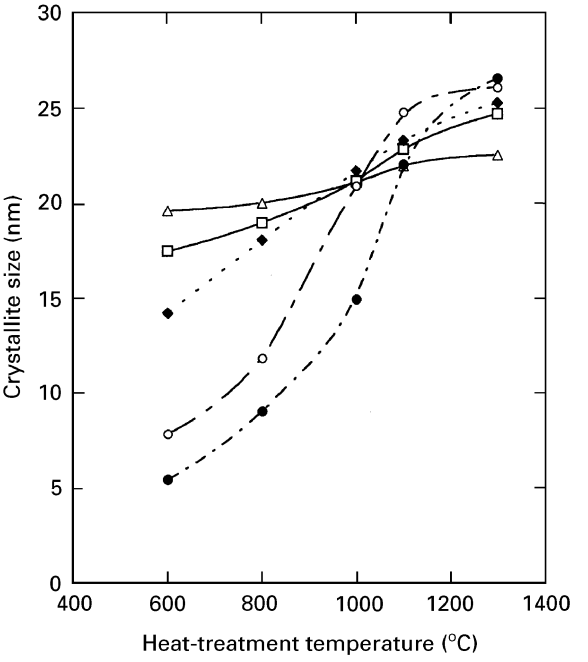

Figure 11 Heat-treatment temperature dependence of the crystallite size of YZ thin film heated for 2 h. The crystallite size was calculated from the (1 1 1) diffraction peak. (△) 2 mol %, (□) 5 mol %, (◆) 8 mol %, (○) 11 mol %, (●) 20 mol %.

Fig. 11 shows the relationship between heat-treatment temperature and crystallite size of YZ thin film heated for 2 h. The crystallite size was calculated from the Scherrer equation by using the (1 1 1) diffraction peak obtained from XRD-LB measurements. The crystallite size of all the thin films used in this study is smaller than the crystal size of 30 nm, above which the metastable tetragonal phase cannot exist at lower temperatures as a result of the crystallite size effect.

The crystallite sizes increase with increasing heat-treatment temperature, and become saturated at 1300 °C. This result indicates that the crystals of the films may be grown up to 1300 °C. It is also shown that the crystallite size at lower temperatures becomes larger with decreasing doping concentration, which is in contrast to the heat-treatment temperature of 1300 °C. This may be responsible for an interference of zirconia crystallization with the existence of yttria, showing that the nuclei formation during crystallization is suppressed by yttria.

The variation of crystallite sizes with the doping concentration at constant temperature reflects the variation of XRD peak intensities, where the peak becomes broad with increasing yttria content, as shown in Fig. 6.

The electrical properties of YZ thin film are discussed. In order to measure the electrical conductivity of materials, the contribution of the electrode resistance at the electrode/material interface must be eliminated. This was effectively achieved with the complex impedance techniques as introduced in this study.

Fig. 12 shows the compositional dependence of electrical conductivity in the system of YZ heat treated at 1300 °C. The conductivity was measured at 600 °C

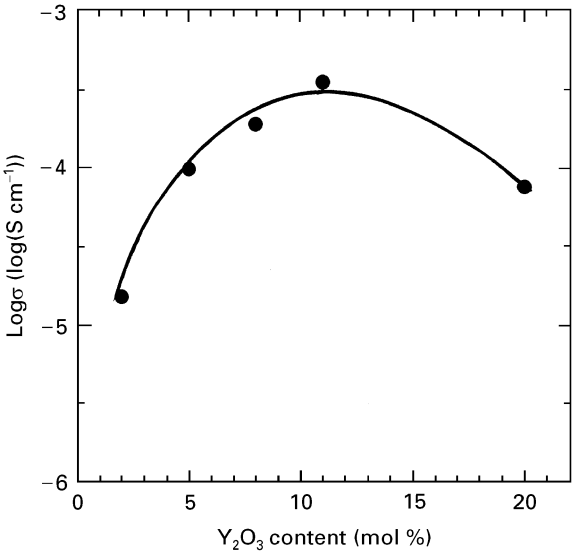

Figure 12 Electrical conductivity of YZ thin film measured at 600 °C in air. The specimens heat treated at 1300 °C for 2 h were used.

in air. The line is drawn as a guide to the eye. $\log\sigma$ ($S\,cm^{-1}$) has a maximum value at around 10 mol %, and then decreases with increasing yttria content. It is known that the location of the conductivity maximum corresponds to the minimum amount of the dopant required to stabilize fully the fluorite phase.

The conductivity of YZ thin films prepared in this study was similar to the values of the sintered body, the single crystal and the plasma-sprayed films reported by Chiodelli *et al.* [21].

According to the general expression $\sigma = \sigma_0 \exp(-\Delta H/RT)$, the variations in $\log\sigma_0$ and the activation energy, ΔH, with the dopant content were obtained from the Arrhenius plots between the conductivity and the measured temperature. The result is characteristic of the tendency for $\log\sigma_0$ to increase with increasing yttria content. The pre-exponential factor, σ_0, is known to be proportional to the carrier concentration and a square of the jumping distance. In this case, the increase in $\log\sigma_0$ can be approximated to the increase of the carrier concentration, because the variation in the jumping distance with the yttria dopant is much smaller than that in the carrier concentration.

Therefore, the increase in the conductivity up to the maximum in the conductivity–dopant concentration curves of Fig. 12 can be explained by the increase in the carrier concentration. Many yttrium cations substitute for Zr^{4+} in the lattice sites and as a result of their lower valence state, they also create more vacancies in the oxygen sublattice.

The decrease in conductivity from a maximum value with increasing yttria content, however, can be explained in terms of a blocking effect of the larger cations. The migration of vacancies is more effectively blocked by larger dopant cations.

The conductivity behaviour in dilute solid solutions and in the high-temperature range, when vacancies are free and mobile, is more easily explained by such models. However, for concentrated solutions in the low-temperature range, vacancies form associates by the coulombic interactions. Thus, the carrier concentration becomes diminished, and then the conductivity is decreased with increasing doping concentration. We cannot discriminate the correct mechanism for this study, but the data of the conductivity behaviour are reasonable.

4. Conclusions

Y_2O_3-doped and ZrO_2 thin films were prepared by the sol–gel process using the dip-coating method. The following conclusions are drawn.

1. A uniform thin film was prepared by using zirconium chloride octahydrate and yttrium chloride hexahydrate as raw materials, with ethylene glycol, 2-butanol and distilled water as solvents.
2. YZ crystalline films were produced by the thermal treatment above 600 °C, at which temperature raw materials were completely decomposed.
3. In all YZ thin films, the tetragonal phase was stable at low temperatures as a result of the crystallite size effect; however, at the higher temperatures the tetragonal phase was transformed into either the monoclinic phase or the cubic phase, depending on the doping concentration. YZ thin film of 8 mol % Y_2O_3 content was stabilized to almost cubic phase at 1000 °C.
4. Reasonable conductivity behaviour at YZ was observed for the YZ thin films. The electrical conductivity of YZ thin films was similar to the values of the sintered body.

References

1. Y. TAKAHASHI, K. NIWA, K. KOBAYASHI and M. MATSUKI, *Yogyo-Kyokai-Shi* **95** (1987) 942.
2. L. YANG and J. CHENG, *J. Non-Crystl. Solids* **112** (1989) 442.
3. K. IZUMI, M. MURAKAMI, T. DEGUCHI and A. MORITA, *J. Amer. Ceram. Soc.* **72** (1989) 1465.
4. P. DE LIMA NETO, M. ATIK, L. A. AVACA and M. A. AEGERTER, *J. Sol-Gel Sci. Technol.* **2** (1994) 529.
5. R. CARUSO, N. PELLEGRI, O. DE SANCTIS, M. C. CARACOCHE and P. C. RIVAS, *ibid.* **3** (1994) 241.
6. M. ATIK, C. R. KHA, P. DE LIMA NETO, L. A. AVACA, M. A. AEGERTER and J. ZARZYCKI, *J. Mater. Sci. Lett.* **14** (1995) 178.
7. A. NEGISHI, *Yogyo-Kyokai-Shi* **93** (1985) 566.
8. M. SHANE and M. L. MECARTNEY, *J. Mater. Sci.* **25** (1990) 1537.
9. R. D. MAGGIO, P. SCARDI and A. TOMASI, *Mater. Res. Soc. Symp. Proc.* **180** (1990) 481.
10. P. PESHEV and V. SLAVOVA, *Mater. Res. Bull.* **27** (1992) 1269.
11. T. W. KUEPER, S. J. VISCO and L. C. DE JONGHE, *Solid State Ionics* **52** (1992) 251.
12. C. SAKURAI, T. FUKUI and M. OKUYAMA, *J. Amer. Ceram. Soc.* **76** (1993) 1061.
13. K. MIYAZAWA, K. SUZUKI and M. Y. WEY, *ibid.* **78** (1995) 347.
14. U. B. PAL and S. C. SINGHAL, *J. Electrochem. Soc.* **137** (1990) 2937.
15. M. C. CAROLAN and J. N. MICHAELS, *Solid State Ionics* **37** (1990) 189.
16. R. C. GARVIE, *J. Phys. Chem.* **69** (1965) 1238.

17. S. RAMANATHAN, R. V. MURALEEDHARAN, S. K. ROY and P. K. K. NAYAR, *J. Amer. Ceram. Soc.* **78** (1995) 429.
18. J. S. LEE, J. I. PARK and T. W. CHOI, *J. Mater. Sci.*, **31** (1996) 2833.
19. T. H. ETSELL and S. N. FLENGAS, *Chem. Rev.* **70** (1970) 339.
20. V. S. STUBICAN, in "Advances in Ceramics", Vol. 24A, edited by S. Sōmiya, N. Yamamoto and H. Yanagida (The American Ceramic Society, Westerville, OH, 1988) p. 71.
21. G. CHIODELLI, A. MAGISTRIS, M. SCAGLIOTTI and F. PARMIGIANI, *J. Mater. Sci.* **23** (1988) 1159.

Received 4 December 1995
and accepted 10 March 1997